Assembly of large-area, highly ordered, crack-free inverse opal films

Benjamin Hatton[a,b], Lidiya Mishchenko[a], Stan Davis[c], Kenneth H. Sandhage[c,d], and Joanna Aizenberg[a,b,1]

[a]School of Engineering and Applied Sciences, Harvard University, Cambridge, MA 02138; [b]Wyss Institute for Biologically Inspired Engineering, Harvard University, Cambridge, MA 02138; [c]School of Materials Science and Engineering, Georgia Institute of Technology, Atlanta, GA 30332; and [d]School of Chemistry and Biochemistry, Georgia Institute of Technology, Atlanta, GA 30332

Edited by Jack Halpern, The University of Chicago, Chicago, IL, and approved April 16, 2010 (received for review January 24, 2010)

Whereas considerable interest exists in self-assembly of well-ordered, porous "inverse opal" structures for optical, electronic, and (bio)chemical applications, uncontrolled defect formation has limited the scale-up and practicality of such approaches. Here we demonstrate a new method for assembling highly ordered, crack-free inverse opal films over a centimeter scale. Multilayered composite colloidal crystal films have been generated via evaporative deposition of polymeric colloidal spheres suspended within a hydrolyzed silicate sol-gel precursor solution. The coassembly of a sacrificial colloidal template with a matrix material avoids the need for liquid infiltration into the preassembled colloidal crystal and minimizes the associated cracking and inhomogeneities of the resulting inverse opal films. We discuss the underlying mechanisms that may account for the formation of large-area defect-free films, their unique preferential growth along the ⟨110⟩ direction and unusual fracture behavior. We demonstrate that this coassembly approach allows the fabrication of hierarchical structures not achievable by conventional methods, such as multilayered films and deposition onto patterned or curved surfaces. These robust SiO_2 inverse opals can be transformed into various materials that retain the morphology and order of the original films, as exemplified by the reactive conversion into Si or TiO_2 replicas. We show that colloidal coassembly is available for a range of organometallic sol-gel and polymer matrix precursors, and represents a simple, low-cost, scalable method for generating high-quality, chemically tailorable inverse opal films for a variety of applications.

coassembly | colloidal assembly | crack-free films | inverse opals | nanoporous

Self-assembly methods have attracted considerable interest as potential alternatives to conventional top-down processes for the scalable, low-cost syntheses of nanoporous solid structures. Examples include the self-assembly of periodic colloidal "opal" templates that, in turn, can direct the infiltration and deposition of functional materials to yield nanoporous "inverse opal" structures (1–5). Inverse opals can exhibit a high degree of interconnected porosity (approximately 75%) with extremely uniform size (average size normally in the range of 100–1000 nm) and periodic distributions of pores, achieved through colloidal monodispersity. Such structures have been shown to be potentially useful in a wide range of fields, including photonics (6–10), tissue engineering (11, 12), sensing (13, 14), and catalysis (10, 15, 16). However, whereas conventional self-assembly has yielded ordered inverse opal structures over modest ($\leq 10\ \mu m$) length scales, such processes have been plagued by uncontrolled formation of defects over larger length scales (2, 3), thus limiting their real-world applications.

Conventional colloidal self-assembly of inverse opal materials (Fig. 1*A*) has generally been conducted in three sequential steps: ***1.*** assembly of a colloidal crystal template (e.g., comprised of polymer latex spheres), ***2.*** infiltration and deposition of a matrix phase, or a precursor to a solid matrix phase, and ***3.*** selective removal of the colloidal crystal template to yield an inverse porous structure (1–5). In the first step, thin film colloidal crystal templates have been produced via sedimentation (1), shear flow (4), spin-coating (17), and evaporative (18–20) or "flow-controlled" deposition (21, 22). The use of these self-assembly processes to form large-area colloidal crystal films has very typically resulted in the formation of cracks, domain boundaries, colloid vacancies, and other defects. Efforts have also been made to inhibit cracking (23) and control domain orientation of colloidal crystal films through changes of evaporative deposition conditions (20, 24), particle presintering (25), and deposition onto topologically patterned substrates (26). In the second step, sol-gel solutions have been used as matrix precursors for the syntheses of porous oxide materials, such as SiO_2, TiO_2, and Al_2O_3 (1–5). Matrices have also been deposited via infiltration of polymer precursors (6, 27), salt precursors (28), nanoparticles (29), or vapor phase precursors (7, 30, 31). Capillary forces generated during drying after self-assembly, or infiltration of the template, have led to additional cracking of these mechanically fragile templates. Efforts to increase the strength of self-assembled templates have been made by partial sintering (32) or growth of necks between spheres (33). Moreover, excessive infiltration and deposition in the second fabrication step results in overlayer formation, whereas incomplete or nonconformal deposition often leads to structural collapse during template removal in the third step. Whereas layer-by-layer vapor phase processes, such as atomic layer deposition, may yield continuous and conformal coatings and avoid the formation of cracks associated with liquid infiltration or drying, these approaches are relatively time consuming and expensive, and still require a defect-free colloidal template to grow upon. No reliable, low-cost, scalable methods have been demonstrated for the synthesis of crack-free, robust inverse opal films comprised of single-crystal domains over large (cm or more) lateral dimensions.

Herein we demonstrate the evaporative coassembly of a sacrificial colloidal template with a matrix material in a single step to yield a colloidal composite, thereby avoiding the need for liquid infiltration into a preassembled porous structure (Fig. 1*B*). Previously, colloidal coassembly of structures has been achieved with binary mixtures of colloids (34–38), supramolecular mesostructures (39), and with a combination of supramolecular and colloidal self-assembly (40). Also, sol-gel silicates have been added as a temporary "glue" for SiO_2 colloids (41). Our approach goes beyond the coassembly of binary colloidal mixtures or a combination of supramolecular and colloidal self-assembly, and relies on polymer colloids [e.g., polystyrene (PS) or poly (methyl methacrylate) (PMMA)] assembling in a broad range

Author contributions: B.H., K.H.S., and J.A. designed research; B.H., L.M., S.D., and J.A. performed research; L.M., B.H., K.H.S., and J.A. analyzed data; and B.H., L.M., K.H.S., and J.A. wrote the paper.

The authors declare no conflict of interest.

This article is a PNAS Direct Submission.

Freely available online through the PNAS open access option.

[1]To whom correspondence should be addressed. E-mail: jaiz@seas.harvard.edu.

This article contains supporting information online at www.pnas.org/lookup/suppl/doi:10.1073/pnas.1000954107/-/DCSupplemental.

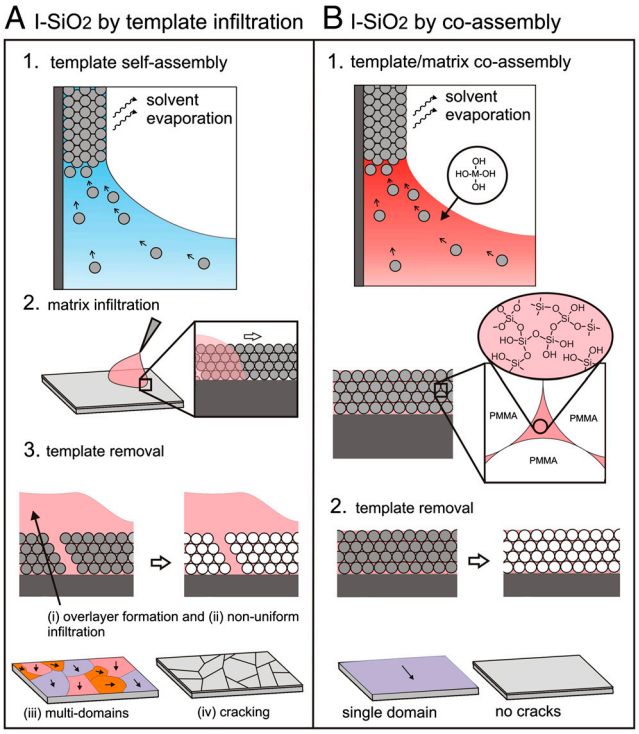

Fig. 1. Schematics of "conventional" colloidal template self-assembly (*A*), and coassembly of colloids with a soluble matrix precursor (*B*), for the syntheses of inverse opal thin films. The conventional method typically involves the sequential steps of colloidal self-assembly, matrix infiltration, and template removal. The use of such conventional colloidal self-assembly to generate large-area films has been plagued with the formation of defects, such as overlayer coatings, multiple domains, and significant cracking. Colloidal coassembly combines the steps of template self-assembly with matrix infiltration into one process in which colloids are allowed to assemble directly from the sol-gel solution, to yield robust inverse opal films with no overlayer, very large (mm to cm) ordered domains, and no cracks, due to the "gluing" action of the sol-gel matrix.

of sol-gel precursor solutions (e.g., $M(OH_4)$, M = Si, Ti, Ge) through an evaporative deposition (18, 19, 42), to form a large-area, defect-free composite opal film. In particular, when PMMA spheres are deposited from a hydrolyzed tetraethoxy silane (TEOS) solution, the resulting structure contains silica gel matrix material, distributed uniformly in the interstitial spaces of the polymeric opal film that, upon firing, yields a high-quality inverse opal silica structure (herein abbreviated as I-SiO_2) ordered over a cm length scale. The robust nature of these nanoporous I-SiO_2 films also allows their direct chemical transformation to porous Si (43, 44) or TiO_2 replicas (45). A range of complex hierarchical and patterned structures coated with inverse opals can be fabricated. Hence, this coassembly approach enables the low-cost, large-area syntheses of ordered, crack-free inverse opal films of tailorable chemistry for a wide variety of applications.

Results and Discussion

Initial experiments on the syntheses of SiO_2/PMMA composite films were conducted with varying amounts of TEOS solution added to suspensions of colloidal PMMA in water, to determine an optimal SiO_2/colloid ratio for well-ordered colloidal deposition. The TEOS-to-colloid ratio was found to have a significant influence on the film structure and defect formation (Fig. S1). Insufficient silicate additions did not allow for the formation of a continuous SiO_2 network throughout the colloidal template, leading to considerable tearing/cracking of the film, similar to that observed for a PMMA colloidal crystal (Fig. 2*A*). However, beyond a critical TEOS content (approximately 0.15 mL TEOS solution per 20 mL PMMA suspension), highly ordered, crack-free films were deposited. Further additions of TEOS to the deposition mixture (>0.20 mL TEOS solution per 20 mL PMMA suspension) caused the initial formation of an overlayer, which increased in thickness with further TEOS additions.

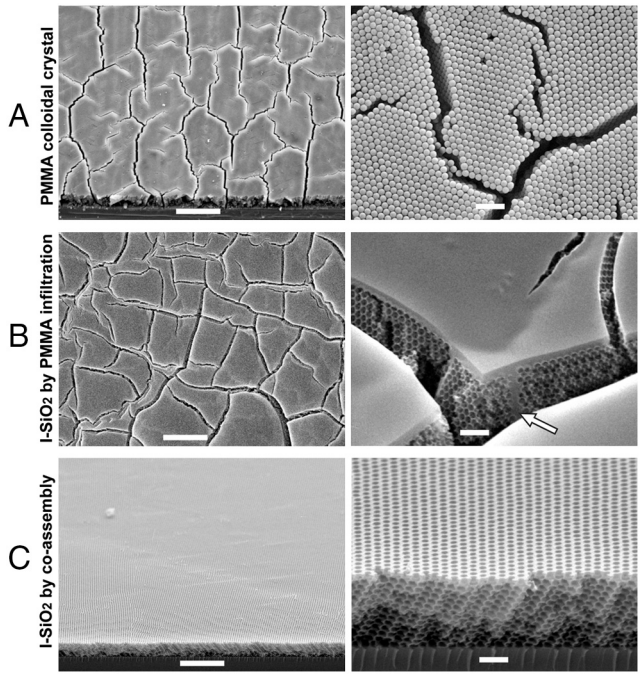

Fig. 2. SEM images of colloidal and inverse opal films. (*A*) PMMA colloidal crystal film (as synthesized), showing cracks propagating along the close-packed {111} planes and spaced at the 5–10 μm scale); (*B*) I-SiO_2 (inverse opal) film by sol-gel infiltration (calcined to remove PMMA template), showing an overlayer coating, cracking in both the inverse opal and overlayer coating, and a region of SiO_2 infiltration into a preexisting template defect (white arrow); (*C*) I-SiO_2 film by PMMA/sol-gel coassembly, showing highly uniform films with no cracks. Note that the thickness of the coassembled film is comparable (and higher) than the thickness of the cracked film shown in (*A*). Left scale bars = 10 μm, right scale bars = 1 μm.

Fig. 2 compares the quality of the coassembled I-SiO_2 films with the PMMA colloidal crystals and I-SiO_2 films generated by infiltration, of approximately the same thickness (3–4 μm). A typical PMMA colloidal crystal deposited by evaporative deposition (from a solution containing no TEOS), shows significant cracking with a characteristic branched pattern at two length scales: (*i*) large, interconnected {111} cracks with an intercrack distance of approximately 10 μm, and (*ii*) microcracks with an intercrack distance of approximately 1–2 μm (Fig. 2*A*). A variety of defects and micron-sized misaligned domains are evident. The infiltration step further reduced the quality of the films due to the formation of an overlayer, partial filling of the cracks developed during the assembly of the template PMMA crystal, and an additional "glassy" crack pattern originated from the overlayer and nonuniform infiltration (Fig. 2*B*). The coassembled I-SiO_2 film (Fig. 2*C*) was produced under the following optimized conditions: (*i*) suspending a vertically oriented glass slide in a mixture comprised of 0.15 mL of a 28.6 wt% TEOS solution with a 20 mL suspension of 280 nm diameter PMMA spheres (approximately 0.125 vol%), (*ii*) allowing the solvent to slowly evaporate at 65 °C (deposition rate = 2 cm/day), and (*iii*) treating the composite structure at 500 °C for 5 h in air. These conditions were found to generate nearly perfect, crack-free inverse opal films.

The film thickness can be controlled by regulating the colloidal volume fraction (for a constant TEOS-to-PMMA ratio). The number of layers increased linearly with colloidal concentration (Fig. 3*A*). No cracks were observed in films with up to approximately 18–20 sphere layers (i.e., thicknesses up to approximately

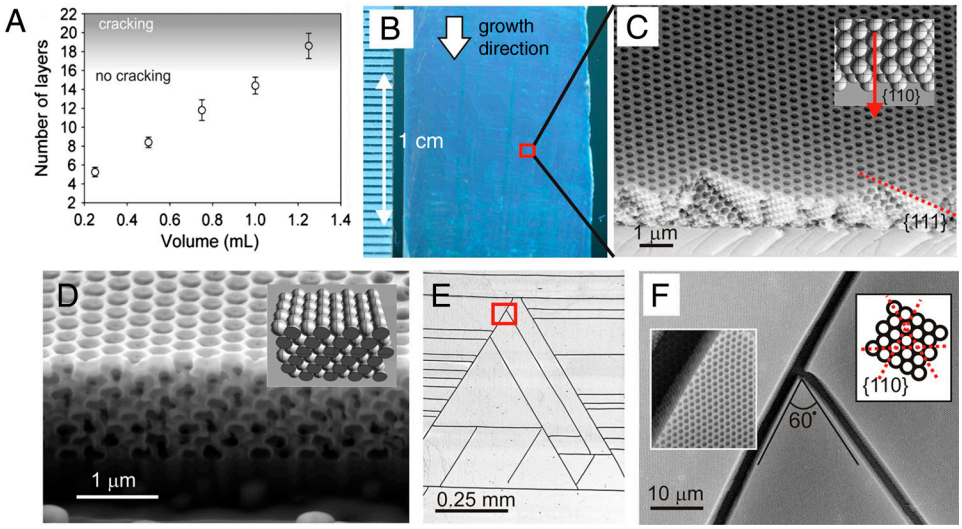

Fig. 3. Well-ordered SiO_2 inverse opal films produced by colloidal coassembly. (*A*) Linear relationship between film thickness (number of sphere layers) and colloidal concentration (volume of PMMA stock solution in 20 mL H_2O), and threshold thickness for crack formation; (*B*) optical photograph of an I-SiO_2 film deposited on glass (substrate width approximately 1.5 cm); (*C*) a fracture cross section of a crack-free I-SiO_2 film on a Si wafer, showing the ⟨110⟩ growth orientation, as illustrated by an fcc model (*Inset*); (*D*) a FIB-cut cross section of a film showing the {110} plane (a model is shown in the inset); (*E*) optical photograph of the triangular crack pattern in a thick I-SiO_2 film; (*F*) SEM image of the corner cracked region indicated in (*E*), with schematic illustration and higher magnification SEM image showing fracture along the {110} planes. All of the films in this figure are oriented with the vertical growth direction aligned from top to bottom.

5 μm). Fig. 3*B* shows an optical micrograph of a film (<20 layers) that has no cracks across the entire substrate length (i.e., 2–3 cm in these experiments). Thin films typically have an upper threshold thickness, beyond which "channel" type cracking occurs (46, 47). Noticeably, sol-gel SiO_2 films tend to fracture at a threshold thickness of approximately 0.5 μm (10× smaller than the coassembled films), and colloidal crystals of similar thickness invariably crack (unless modified in some way) (6, 11, 24, 25, 28–31) (Fig. 2*A*). Coassembled films with >20 layers begin to develop cracks (Fig. 3 *C* and *D*), but their characteristic triangular fracture is qualitatively different from the irregular, tortuous crack patterns in colloidal crystals. In particular, the distance between the cracks was in the order of approximately 100 μm with no microcracks, thus producing defect-free regions that are 100× larger than those in the conventional films (Fig. 2 *A* and *B*). Higher magnification SEM images in Figs. 2*C* and 3 *C* and *D* reveal the ordered and defect-free nature of the coassembled films.

As previously reported for evaporative deposition, the films had a fcc structure, with the {111} plane oriented parallel to the surface (1–5, 17–22, 32–41, 48). We observed that the composite films always selectively grow along the ⟨110⟩ direction of the deposited fcc structure, as indicated in Fig. 3*C*. Interestingly, under conditions of slow conventional growth for colloidal crystals, the ⟨112⟩ growth orientation is expected to dominate the ⟨110⟩ orientation (48). Under our conditions, the strong preference for the ⟨110⟩ orientation (Fig. 3 *C* and *D*) was made particularly evident by a unique defect "self-healing" phenomenon (Fig. S2). Domains that occasionally nucleate and grow with a different orientation gradually become "corrected" to the default ⟨110⟩ orientation, and the defect eventually disappears. Because this kind of defect correction and preferred direction of growth have not been previously reported in the conventional deposition of colloidal crystals, it is apparent that the silicate additions induce the preferential growth in the ⟨110⟩ direction and help to increase the order of the resulting films. Such TEOS-enhanced ordering yields ⟨110⟩-oriented films with single domains extending over the cm scale, 3–4 orders of magnitude larger than have been reported for conventional colloidal crystals (and, by extension, inverse opals derived from them) without the use of patterned substrates or external fields (24, 26) (Fig. 2).

We have observed that two different fracture directions are present in the coassembled films as a function of the film thickness. Cracks in fcc colloidal crystal films typically occur along the close-packed {111} planes, which represent the planes of weakness (49) (Fig. 2*A*). For an inverse opal structure, the {111} planes represent the highest pore density, and thus are the obvious candidates for crack propagation. Indeed, thin (<5 μm) crack-free I-SiO_2 films reveal the expected {111} fracture when cleaved intentionally (Figs. 2*C* and 3*C*). However, cracks in thick films (>5 μm) show an unexpected, unique orientation along {110} planes of the colloidal crystal (Fig. 3 *E* and *F*). It is noteworthy that the preference for a vertical orientation of tortuous cracks has been predicted and observed in vertically grown colloidal crystals (50). However, no such cracks develop for our (thick) I-SiO_2 films, instead revealing straight fracture lines running along the {110} planes; i.e., horizontally and at 30° to the vertical direction. We believe that these cracks develop during the coassembly of colloids with the silica gel and therefore reflect the unique fracture mechanics of a more complex, composite opal/matrix system. These cracks extend uniformly across the entire length of the samples (2–3 cm), indicating the presence of a single crystalline domain.

Our results clearly indicate that in addition to the reduction of the synthetic steps involved in the fabrication of inverse opal films, the colloid/matrix coassembly process described here offers significant improvement of the quality of the films. Cracking of conventional opal and inverse opal films tends to occur upon drying both at the colloidal assembly stage and at the infiltration stage due to a combination of dehydration and/or polymerization-induced contraction and associated local capillary forces (23, 46). The sol-gel matrix that undergoes polycondensation at the time of colloidal assembly provides a glue/necking to the assembling spheres. The thin-walled (approximately 30 nm thick), interconnected silicate network in these coassembled composite films inhibits the formation/propagation of cracks for film thicknesses up to approximately 5 μm. Whereas the detailed mechanism of this unique crack-free growth is being currently investigated, we propose that the process might be similar to the formation of large single crystals of calcite patterned at the micron scale (51, 52). In the latter case, the transformation of the amorphous $CaCO_3$ film into a defect-free, porous calcite

crystal is facilitated by the micropatterned substrate that not only determines the pattern of porosity of the final single crystal, but also provides interfacial sites for stress and impurity release during the amorphous-to-crystalline transition. Similarly in the current system, the formation of a colloidal crystal and the associated interfaces between the polymerizing sol-gel solution and the assembling colloidal spheres may provide sites for the relaxation of tensile stresses encountered during the gelation process. Controlled solvent release during the polycondensation reaction can also occur at these interfaces and be channeled through the interconnected porous network to evaporate at the surface.

The direct combination of the colloidal template and matrix gives this method a great versatility for the fabrication of inverse opal layers in structures and applications not practically possible by conventional methods. Fig. 4 shows representative examples of such complex, hierarchical materials. Multilayer inverse opal structures with varying pore sizes can be created by the successive deposition of template/matrix composite layers (Fig. 4*A*). Such structures could have important applications in differential drug release, where sequential dosed release of components can be achieved by selective pore size engineering due to the differences in the rate of desorption and diffusion. The exceptional ordering in this coassembly process can be utilized for depositing inverse opal films onto patterned substrates (Fig. 4*B*), making them well suited for microfluidics, optical and photonic devices, or sensors (53). Finally, coassembly can be used to deposit inverse opals

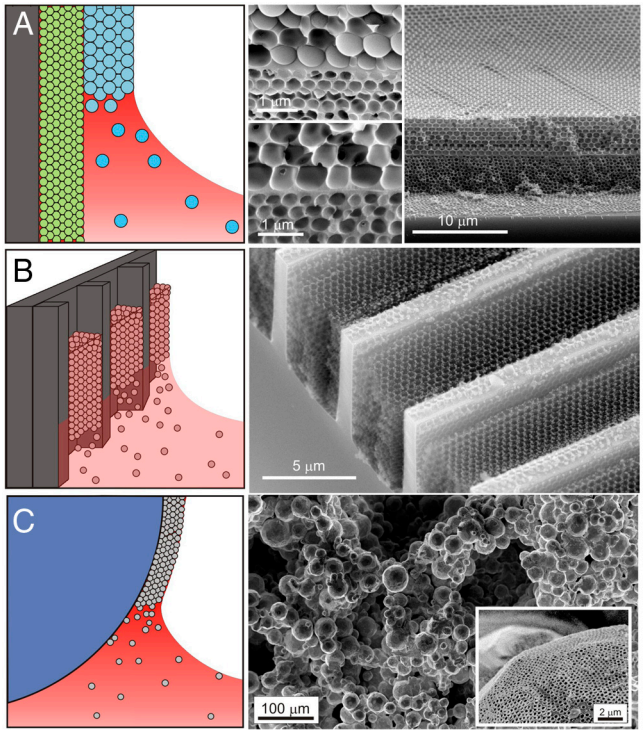

Fig. 4. Novel SiO_2 inverse opal structures enabled by colloidal coassembly. Schematics of the processes are shown on the left and the representative SEM images are shown on the right. (*A*) Schematic presentation of the synthesis of multilayered, hierarchical films with different pore sizes by successive layer deposition prior to template removal (*Left*), and a SEM cross section images of a bilayer SiO_2 structure produced using 300 nm and 720 nm colloidal spheres (*Right*). The top left and bottom left SEM images show the interface between layers before and after calcination, respectively. (*B*) Schematic presentation of the oriented SiO_2 structures grown on topologically patterned substrates (*Left*), and an SEM fractured cross section of inverse opals grown in 4 μm wide, 5 μm deep channels on a Si substrate (*Right*). (*C*) Schematic presentation of the coassembly onto curved surfaces (*Left*), and SEM images (*Right*) of a SiO_2 inverse opal film layer (shown magnified, *Inset*) deposited onto a sintered, macroporous Ti scaffold structure.

onto arbitrarily shaped substrates, such as curved surfaces. Fig. 4*C* shows Ti beads coated with an I-SiO_2 layer. Such high-surface area, hierarchical assemblies could have important applications for catalysis and biomedical surfaces.

Whereas silicate/polymer colloidal coassembly is an important demonstration of ordered, defect-free films, SiO_2 itself has limited useful chemical and physical properties. The properties of porous SiO_2 structures may be expanded by binding a wide variety of functional molecules to SiO_2 surfaces (54). We have also explored the coassembly method to form inverse opal films using other precursor materials, such as organosilica ($SiO(C_2H_4)$), with an ethane-bridged silsesquioxane, and TiO_2 with a water-soluble TiO_2 precursor (TiBALDH) (Fig. S3). An alternate approach for expanding the range of chemistries and associated properties is to utilize shape-preserving gas/solid reactions to directly convert the I-SiO_2 films into other materials. To evaluate whether such reactive conversion approaches maintain the structure of coassembled I-SiO_2 films, we have examined the direct chemical transformation of these structures into Si (43, 44) and TiO_2 (45).

The conversion of coassembled I-SiO_2 films into Si inverse opals was conducted via a "magnesiothermic" reaction with Mg vapor to generate a cocontinuous Si/MgO nanocomposite (43). The MgO phase was then selectively removed to produce a highly porous Si structure. SEM and transmission electron miscroscope (TEM) analyses of a starting I-SiO_2 film, a Si/MgO-converted composite, and a final Si-converted inverse opal are shown in Fig. 5 *A–C*, respectively. The Si/MgO-converted film retained an ordered structure, and no additional cracks formed. The Si/MgO-composite exhibited a modest (approximately 10%) contraction in the direction normal to the film, relative to the starting I-SiO_2 film, however. Selective dissolution of the MgO yielded the Si inverse opal film. Selected area electron diffraction (SAED) analysis (Fig. 5*C*) revealed only the presence of Si, although small amounts of residual (undissolved) Mg and O were detected by energy dispersive spectroscopy (EDS) (Fig. S4). High resolution TEM imaging indicated that the Si/MgO and Si inverse opal films are composed of 5–10 nm nanocrystals.

The conversion of the coassembled I-SiO_2 films into TiO_2 inverse opals was conducted via a metathetic displacement reaction with TiF_4 (45). SEM and TEM images of the resulting TiO_2 inverse opal product (Fig. 5*D*) indicate that the periodic porous structure is very well maintained after reaction. Whereas minor cracking of the films did occur in this case, further optimization of the reaction conditions is underway to determine if such cracking may be avoided. The SAED pattern of the converted film is consistent with anatase. The high resolution TEM image in Fig. 5*D* also reveals lattice fringes of the fine anatase nanocrystals (in the 10–20 nm range), with a spacing (0.36 nm) corresponding to the {101} planes. Further annealing at 900 °C resulted in conversion of anatase into rutile titania, whereas maintaining the inverse opal structure. TiO_2 has important optical, catalytic, and photochemical properties that make it particularly attractive as an inverse opal film material (2, 9, 15). The optical spectra of a film before and after conversion to TiO_2 clearly show a red-shift in the Bragg peak from 460 to 589 nm, corresponding to an increase in refractive index (Fig. S5).

In summary, we have demonstrated synthesis of crack-free, highly ordered inverse opal films over cm length scales by a simple, two-step, solution-based colloidal/matrix coassembly process. Major advantages of this approach include: (*i*) a great reduction in the defect population (particularly crack density), (*ii*) the growth of large, highly ordered domains via a scalable process, (*iii*) prevention of overlayer formation and nonuniform infiltration, (*iv*) minimizing the number of fabrication steps (i.e., avoidance of postassembly infiltration provides a time/cost/quality advantage), and (*v*) the ability to form multilayered, hierarchical, patterned, and curved film structures that are not easily possible by any other method. Furthermore, we have demonstrated that

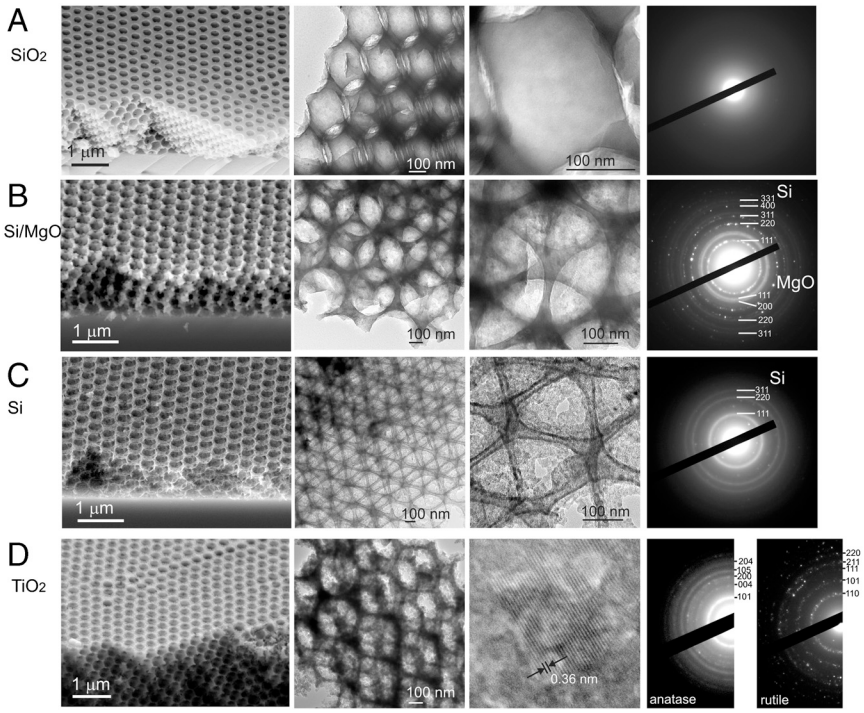

Fig. 5. Morphology-preserving reactive transformation of inverse opal SiO_2 films into MgO/Si, Si, and TiO_2. SEM images (left column), TEM images (center two columns), and SAED analysis (right column) are shown for: (*A*) a starting I-SiO_2 film, (*B*) a Si/MgO replica after reaction with Mg(g) at 850 °C for 4 h, (*C*) a Si replica film after selective MgO dissolution, and (*D*) a TiO_2 replica film after reaction with TiF_4(g) at 200 °C for 2 h and with water vapor at 400 °C for 5 h.

these SiO_2 inverse opal films are sufficiently robust and homogeneous to allow direct conversion, via morphology-preserving gas/solid displacement reactions, into inverse opal films comprised of other materials (e.g., porous Si and TiO_2). We discussed the assembly mechanisms that underlie the unusual characteristic features of the coassembled inverse opal films, such as their preferred crystallographic orientation, the absence of defects and remarkable atypical orientations of the crack patterns, which all pose interesting fundamental questions in soft condensed matter and fracture mechanics. This scalable route to highly ordered, large-area, chemically tailorable inverse opal films may be utilized in a diverse range of applications. Due to the absence of an overlayer, the high porosity of the coassembled films is readily accessible from the top surface, which is especially important for applications in catalysis (10, 15, 16), gas adsorption (55), or tissue engineering (11, 12). These single-domain periodic inverse opal films can also behave as large-area photonic band gap structures for applications in photonics (6–10).

Methods

Monodispersed colloidal particles of PMMA or PS (250–400 nm diameter, approximately 3% standard deviation) were synthesized by surfactant-free emulsion polymerization using an ammonium persulfate initiator (56), or were purchased commercially (IDC/Invitrogen). 1.0 mL of a 2.5 vol% "stock" colloidal suspension (cleaned by centrifugation) was added to 20 mL of distilled/DI H_2O, and *x* mL of added hydrolyzed TEOS solution, where *x* was varied from 0 to 0.30 mL. The standard TEOS solution consisted of 1:1:1.5 ratio by weight of TEOS (98% Aldrich), 0.10 M HCl, and EtOH (100%), respectively, stirred at room temperature for 1 h prior to use. Glass or Si substrates (approximately 1×4 cm), cleaned in piranha solution, were vertically suspended in the vial containing the colloid/TEOS suspension. The solvent content was evaporated slowly over a period of 1–2 d in a 65 °C oven on a pneumatic vibration-free table, to allow the deposition of a thin film onto the suspended substrate (growing approximately 2 cm/day). The films were then fired in air at 500 °C for 2 h, with a 4 h ramp time (ThermoScientific), to remove the polymer template and partially sinter the SiO_2 structure.

An organosilica silsequioxane precursor (BTES, 1,2-Bis(triethoxysilyl) ethane, Sigma-Aldrich, 96%) and TiBALDH (titanium(IV)- bis-lactato-bis-ammonium dihydroxide, 25% solution, Sigma–Aldrich), a water-soluble TiO_2 precursor, were used as substitutes for the TEOS in solution (in molar ratios equivalent to TEOS), and deposited onto substrates in identical conditions described above. For example, 0.14 mL of 10% TiBALDH solution, or 0.15 mL of a BTES solution (1.7 g BTES, 2.0 g HCl (0.10 M), 3.0 g EtOH), was added to 1.0 mL of the 2.5 vol% PMMA stock suspension in 20 mL DI H_2O. The organosilica and TiBALDH films were calcined at 400 °C and 750 °C in air, respectively. Reactive (magnesiothermic) conversion of the I-SiO_2 films into Si/MgO was achieved by sealing an I-SiO_2 film on Si wafer with a solid Mg vapor source (Alfa Aesar), inside a steel ampoule, in an Ar atmosphere (43). The ampoule was heated at a rate of 5 °C/ min to 850 °C and held at this temperature for 4 h to allow for conversion of the I-SiO_2 film into a Si/MgO composite film. After cooling and removal from the steel ampoule, the reacted film was immersed in a stirred 0.10 M HCl solution at 70 °C for 3 h to selectively dissolve the MgO product to yield a porous Si inverse opal film. For conversion into TiO_2 (45), an I-SiO_2 film was placed in a nickel boat and then sealed, with a solid TiF_4 vapor source (Alfa Aesar), inside a Ti ampoule in an Ar atmosphere. The ampoule was heated at 5 °C/ min to 200 °C and held for 2 h to allow for conversion of the SiO_2 into $TiOF_2$. After cooling and removal from the ampoule, the reacted film was exposed to flowing H_2O vapor in oxygen (generated by passing oxygen through a water bath heated to 60 °C) at 400 °C for 5 h to remove fluorine, and allow for full conversion into an anatase TiO_2 inverse opal film (45).

Optical spectra were taken in reflectance mode using a microscope-based fiber optic spectrometer system (Ocean Optics USB2000+) on a Leica DMRX microscope using a 10× objective. Film structures were imaged by SEM (Zeiss Ultra) at 10 kV after Pt/Pd-sputtering, and TEM (JEOL 2100) at 200 kV on fragments of the films deposited onto Formvar-coated Cu grids (EMS).

ACKNOWLEDGMENTS. This project was supported by the Office of Naval Research under Award N00014-07-1-0690-DOD35CAP and by the Air Force Office of Scientific Research under Award FA9550-09-1-0669-DOD35CAP. The work was performed in part at the Center for Nanoscale Systems (CNS), a member of the National Nanotechnology Infrastructure Network (NNIN), which is supported by the National Science Foundation under Award ECS-0335765. L.M. thanks the US Department of Homeland Security (DHS) for the fellowship. The DHS Scholarship and Fellowship Program is administered by the Oak Ridge Institute for Science and Education (ORISE) through an interagency agreement between the US Department of Energy (DOE) and DHS. ORISE is managed by Oak Ridge Associated Universities (ORAU) under DOE Contract DE-AC05-06OR23100.

1. Holland BT, Blanford CF, Stein A (1998) Synthesis of macroporous minerals with highly ordered three-dimensional arrays of spheroidal voids. *Science* 281:538–540.
2. Lytle JC, Stein A (2006) Recent progress in synthesis and applications of inverse opals and related macroporous materials prepared by colloidal crystal templating. *Ann Rev Nano Res*, eds G Cao and CJ Brinker (World Scientific, Teaneck, NJ), 1, pp 1–79.
3. Velev OD, Lenhoff AM (2000) Colloidal crystals as templates for porous materials. *Curr Opin Colloid Interface Sci* 5:56–63.
4. Xia Y, Gates B, Yin Y, Lu Y (2000) Monodispersed colloidal spheres: old materials with new applications. *Adv Mater* 12:693–713.
5. Zhao XS, et al. (2006) Templating methods for preparation of porous structures. *J Mater Chem* 16:637–648.
6. Arsenault AC, et al. (2006) From colour fingerprinting to the control of photoluminescence in elastic photonic crystals. *Nat Mater* 5:179–184.
7. Blanco A, et al. (2000) Large-scale synthesis of a silicon photonic crystal with a complete three-dimensional bandgap near 1.5 micrometres. *Nature* 405:437–440.
8. Rinnie SA, Garcia-Santamaria F, Braun PV (2008) Embedded cavities and waveguides in three-dimensional silicon photonic crystals. *Nat Photonics* 2:52–56.
9. Eun Sik K, Wonmok L, Nam-Gyu P, Junkyung K, Hyunjung L (2009) Compact inverse-opal electrode using non-aggregated TiO2 nanoparticles for dye-sensitized solar cells. *Adv Funct Mater* 19(7):1093–1099.
10. Chen JIL, von Freymann G, Choi SY, Kitaev V, Ozin GA (2008) Slow photons in the fast lane in chemistry. *J Mater Chem* 18:369–373.
11. Lee J, Shanbhag S, Kotov NA (2006) Inverted colloidal crystals as three-dimensional microenvironments for cellular co-cultures. *J Mater Chem* 16:3558–3564.
12. Sung-Wook C, Jingwei X, Younan X (2009) Chitosan-based inverse opals: Three-dimensional scaffolds with uniform pore structures for cell culture. *Adv Mater* 21:2997–3001.
13. Lee K, Asher SA (2000) Photonic crystal chemical sensors: pH and ionic strength. *J Am Chem Soc* 122:9534–9537.
14. Lee Y-J, Pruzinsky SA, Braun PV (2004) Glucose-sensitive inverse opal hydrogels: Analysis of optical diffraction response. *Langmuir* 20:3096–3106.
15. Ren M, Ravikrishna R, Valsaraj KT (2006) Photocatalytic degradation of gaseous organic species on photonic band-gap titania. *Environ Sci Technol* 40:7029–7033.
16. Guan G, et al. (2008) Preferential CO oxidation over catalysts with well-defined inverse opal structure in microchannels. *Int J Hydrogen Energ* 33:797–801.
17. Jiang P, McFarland MJ (2004) Large-scale fabrication of wafer-size colloidal crystals, macroporous polymers, and nanocomposites by spin-coating. *J Am Chem Soc* 42:13778–13786.
18. Dimitrov AS, Nagayama K (1996) Continuous convective assembling of fine particles into two-dimensional arrays on solid surfaces. *Langmuir* 12:1303–1311.
19. Jiang P, Bertone JF, Hwang KS, Colvin VL (1999) Single-crystal colloidal multilayers of controlled thickness. *Chem Mater* 11:2132–2140.
20. Wong S, Kitaev V, Ozin GA (2003) Colloidal crystal films: Advances in universality and perfection. *J Am Chem Soc* 125:15589–15598.
21. Gu Z, Fujishima A, Sato O (2002) Fabrication of high-quality opal films with controllable thickness. *Chem Mater* 14:760–765.
22. Zhou ZC, Zhao XS (2005) Opal and inverse opal fabricated with a flow-controlled vertical deposition method. *Langmuir* 21:4717–4723.
23. Tirumkudulu MS, Russel WB (2005) Cracking in drying latex films. *Langmuir* 21:4938–4948.
24. McLachlan MA, Johnson NP, De La Rue RM, McComb DW (2004) Thin film photonic crystals: Synthesis and characterisation. *J Mater Chem* 14:144–150.
25. Chabanov AA, Jun Y, Norris DJ (2004) Avoiding cracks in self-assembled photonic band-gap crystals. *Appl Phys Lett* 84:3573–3575.
26. Dziomkina NV, Vancso GJ (2005) Colloidal crystal assembly on topologically patterned templates. *Soft Matter* 1:265–279.
27. Johnson SA, Ollivier PJ, Mallouk TE (1999) Ordered mesoporous polymers of tunable pore size from colloidal silica templates. *Science* 283:963–965.
28. Yan H, Blanford CF, Smyrl WH, Stein A (2000) Preparation and structure of 3D ordered macroporous alloys by PMMA colloidal crystal templating. *Chem Commun* 1477–1478.
29. Shimmin RG, Vajtai R, Siegel RW, Braun PV (2007) Room-temperature assembly of germanium photonic crystals through colloidal crystal templating. *Chem Mater* 19:2102–2107.
30. King JS, Heineman D, Graungnard E, Summers CJ (2005) Atomic layer deposition in porous structures: 3D photonic crystals. *Appl Surf Sci* 244:511–516.
31. Rugge A, Becker JS, Gordon RG, Tolbert SH (2003) Tungsten nitride inverse opals by atomic layer deposition. *Nano Lett* 3:1293–1297.
32. Míguez H, et al. (1998) Control of the photonic crystal properties of fcc packed submicron SiO_2 spheres by sintering. *Adv Mater* 10:480–483.
33. Miguez H, et al. (2002) Mechanical stability enhancement by pore size and connectivity control in colloidal crystals by layer-by-layer growth of oxide. *Chem Commun* 2736–2737.
34. Wang D, Salgueirino-Maceira V, Liz-Marzan LM, Caruso F (2002) Gold-silica inverse opals by colloidal crystal templating. *Adv Mater* 14:908–912.
35. Wang J, et al. (2008) Structural and optical characterization of 3D binary colloidal crystal and inverse opal films prepared by direct co-deposition. *J Mater Chem* 18:981–988.
36. Kitaev V, Ozin GA (2003) Self-assembled surface patterns of binary colloidal crystals. *Adv Mater* 15:75–78.
37. Dinsmore AD, Yodh AG, Pine DJ (1995) Phase diagrams of nearly hard-sphere binary colloids. *Phys Rev E* 52:4045–4057.
38. Subramania G, Constant K, Biswas R, Sigalas MM, Ho K-M (1999) Optical photonic crystals synthesized from colloidal systems of polystyrene spheres and nanocrystalline titania. *J Lightwave Technol* 17:1970–1974.
39. Brinker CJ, Lu Y, Sellinger A, Fan H (1999) Evaporation-induced self-assembly: Nanostructures made easy. *Adv Mater* 11:579–585.
40. Sel O, et al. (2007) Periodically ordered meso- and macroporous SiO2 thin films and their induced electrochemical activity as a function of pore hierarchy. *Adv Funct Mater* 17:3241–3250.
41. Wang L, Zhao XS (2007) Fabrication of crack-free colloidal crystals using a modified vertical deposition method. *J Phys Chem C* 111:8538–8542.
42. Norris DJ, Arlinghaus EG, Meng L, Heiny R, Scriven LE (2004) Opaline photonic crystals: How does self-assembly work?. *Adv Mater* 16:1393–1399.
43. Bao Z, et al. (2007) Chemical reduction of three-dimensional silica micro-assemblies into microporous silicon replicas. *Nature* 446:172–175.
44. Richman EK, Kang CB, Brezesinski T, Tolbert SH (2008) Ordered mesoporous silicon through magnesium reduction of polymer templated silica thin films. *Nano Lett* 8:3075–3079.
45. Lee S.-J, Shian S, Huang Ch-H, Sandhage KH (2007) Rapid, non-photocatalytic destruction of organophosphorous esters induced by nanostructured titania-based replicas of diatom microshells. *J Am Ceram Soc* 90:1632–1636.
46. Brinker CJ, Scherer GW (1990) *Sol-Gel Science: The Physics and Chemistry of Sol-Gel Processing* (Academic, New York).
47. Hutchinson JW, Suo Z (1992) Mixed mode cracking in layered materials. *Adv Appl Mech* 29:63–191.
48. Ishii M, Harada M, Nakamura H (2007) In situ observations of the self-assembling process of colloidal crystalline arrays. *Soft Matter* 3:872–876.
49. Lawn B, Wilshaw TR (1993) *Fracture of brittle solids* (Cambridge University Press, Cambridge, UK).
50. Dufresne ER, et al. (2006) Dynamics of fracture in drying suspensions. *Langmuir* 22:7144–7147.
51. Aizenberg J, Muller DA, Grazul JL, Hamann DR (2003) Direct fabrication of large micropatterned single crystals. *Science* 299:1205–1208.
52. Fratzl P, Fischer FD, Svoboda J, Aizenberg J (2010) A kinetic model of the transformation of a micropatterned amorphous precursor into a porous single crystal. *Acta Biomater* 6:1001–1005.
53. Yang SM, Miguez H, Ozin GA (2002) Opal circuits of light—Planarized microphotonic crystal chips. *Adv Funct Mater* 12:425–431.
54. Hair ML, Tripp CP (1995) Alkylchlorosilane reactions at the silica surface. *Colloid Surface A* 105:95–103.
55. Kang S, Yu J-S, Kruk M, Jaroniec M (2002) Synthesis of an ordered macroporous carbon with 62 nm spherical pores that exhibit unique gas adsorption properties. *Chem Commun* 1670–1671.
56. Goodwin JW, Hearn J, Ho CC, Ottewill RH (1973) Studies on the preparation and characterisation of monodisperse polystyrene latices. *Colloid Polym Sci* 252:464–471.